Semiconductor Science and Technology

PAPER

A study on GaN-based betavoltaic batteries

To cite this article: A Toprak *et al* 2022 *Semicond. Sci. Technol.* **37** 125005

View the article online for updates and enhancements.

You may also like

- Uncovering the non-radiative thermal characteristics of a passive radiative cooler under real operating conditions
Hasan Kocer, Yilmaz Durna, Halil Isik et al.
- Self-consistent scattering analysis of $Al_{0.2}Ga_{0.8}N$/AlN/GaN/AlN heterostructures grown on 6H-SiC substrates using photo-Hall effect measurements
S B Lisesivdin, E Arslan, M Kasap et al.
- Metamaterials with negative permeability and negative refractive index: experiments and simulations
Ekmel Ozbay, Kaan Guven and Koray Aydin

This content was downloaded from IP address 139.179.72.205 on 28/02/2023 at 13:50

Semicond. Sci. Technol. 37 (2022) 125005 (7pp) https://doi.org/10.1088/1361-6641/ac9698

A study on GaN-based betavoltaic batteries

A Toprak[1,*], D Yılmaz[1] and E Özbay[1,2,3]

[1] Nanotechnology Research Center, Bilkent University, 06800 Ankara, Turkey
[2] Department of Electrical and Electronics Engineering, Bilkent University, 06800 Ankara, Turkey
[3] Department of Physics, Bilkent University, 06800 Ankara, Turkey

E-mail: atoprak@bilkent.edu.tr

Received 18 July 2022, revised 2 September 2022
Accepted for publication 30 September 2022
Published 27 October 2022

Abstract

In this paper, a GaN-based betavoltaic epitaxial structure was grown by metal–organic chemical vapor deposition and a p-type ohmic contact was studied for different Ni/Au metal thickness ratios, temperature dependent in N_2:O_2 (1:1) gas atmosphere and different surface treatments for this epitaxial structure. Transfer length method measurements were done after each different process condition in order to check specific contact resistivities. GaN-based betavoltaic batteries were fabricated and a scanning electron microscope (SEM) was used as an electron source to test these devices. For this purpose, devices connected to a printed circuit board were exposed to an electron current of 1.5 nA with 17 keV energy in the SEM. For 1×1 mm^2 devices, a dark current value of 2.8 pA at 0 V, fill factor of 0.35, maximum power conversion efficiency of 3.92%, and maximum output power of 1 μW were obtained.

Keywords: GaN, betavoltaic, batteries

(Some figures may appear in colour only in the online journal)

1. Introduction

GaN-based devices have attracted much attention for high frequency and high power radio frequency (RF) device applications [1, 2], optoelectronic devices [3, 4] and detectors for nuclear radiations [5–9], due to their highly demanded physical and electrical properties, such as wide bandwidth, high saturated electron drift velocity, high breakdown electric field, hard radiation resistance, high responsivity, high detectivity, very low leakage and noise levels.

The operation of a nuclear battery is very similar to that of a p–n junction solar cell and converts a portion of the energy carried by charged particles into electric energy. The first report on a nuclear battery was given by Ehrenberg *et al* in 1951 by describing the electro-voltaic effect. They bombarded the selenium photocells with an electron beam and observed an increase in current [10]. After this work, a method was reported by Ohmart in the same year that allows the generation of electric current from radioactivity [11].

With developments in the field of micro-electromechanical systems (MEMSs), the micro and nano energy requirements in this field have started to increase. Nuclear batteries have become a research hotspot in the field of powering MEMS devices due to their long lifetime, high energy density, insensitivity to climate and temperature, excellent anti-interference ability, small size, light weight, easy miniaturization and integration [9, 12–19].

Theoretical studies show that the conversion efficiency of a betavoltaic nuclear battery increases further as the semiconductor bandwidth increases [9, 20]. GaN materials have a large, adjustable band gap, good electron transport performance, hard radiation resistance, strong thermal stability, high thermal conductivity, stable chemical properties and high conversion efficiency, and these advantages make GaN materials superior to materials such as Si, GaAs, GaP and SiC [14, 19].

As in all detector structures, the efficiency and output power in betavoltaic devices are related to the epitaxial structure and the collection of particles desired to be detected with maximum efficiency. For this, the p-contact layer, which collects the charge carrier particles produced by a nuclear beta source in the active area of the epitaxial structure in betavoltaic

* Author to whom any correspondence should be addressed.

© 2022 IOP Publishing Ltd

devices, must be compatible with the p-GaN layer so as not to form leaks and must have low specific contact resistivity so as not to create heat losses in it. A p-type contact structure with low contact resistance compatible with the p-GaN layer will reduce losses and leakages and increase the conversion efficiency and output power in GaN-based nuclear batteries [21]. However, one of the problems in GaN-based nuclear devices is the difficulty of forming a p-type contact layer with low specific contact resistivity compatible with the p-GaN layer; studies on this subject are still ongoing [22]. Although there are many contact studies on p-GaN in the literature, the mentioned contacts may not be compatible with the epitaxial structure or may give very different results than expected. It was investigated, for the epitaxial structure grown within the scope of this study, how different surface treatments and various metal ratios of Ni/Au at different annealing temperatures affect the ohmic behavior. This was studied in a one-to-one N_2:O_2 (1:1) gas atmosphere depending on the temperature and its effect on p-type ohmic behavior was examined.

During annealing, oxygen boosts the Ga outdiffusion and forms Ga–O compounds at the interface. This causes the surface Fermi level to shift toward the valence band and reduces the contact resistivity. However, high O content can be used to form more N vacancies and/or oxidize the defects on the surface of the p-GaN layer to cause high-resistance surface formations [22, 23]. In addition, studies have shown that using a mixed ambient of N_2 and O_2 achieves better activation of Mg acceptors in the p-GaN (Mg:GaN) layer and this reduces the resistivity of the p-GaN layer [24]. For this reason, within the scope of this study, the ratio of N_2 and O_2 gases was kept equal and its effect on the contact resistance was examined.

In order to test the performance of the GaN-based betavoltaic epitaxial structure we grew and the p-contact we developed, betavoltaic battery fabrication was carried out. However, the difficulty of finding a nuclear beta source and working with it remains the biggest obstacle to the progress, development and spread of such studies to a wider area. To find an alternative solution to this problem and help developments to be made in this area, a scanning electron microscope (SEM) was used as an electron source to test betavoltaic devices within the scope of this study. Using the measurement method emphasized in this study, the aim was to allow the development of nuclear epitaxial structures before testing with a nuclear beta source.

2. Experimental procedure

The GaN-based betavoltaic epitaxial structure was grown on a 2′′ sapphire (Al_2O_3) substrate in a low-pressure metal–organic chemical vapor deposition reactor (Aixtron 200/4 RF-S). Trimethylgallium (TMGa), bis-cyclopentadienyl magnesium (Cp_2Mg), ammonia (NH_3), and silane (SiH_4) were used as Ga, Mg, N, and Si precursors, respectively. The growth of the sample was initiated with a 50 nm GaN nucleation layer at 550 °C and 200 mbar pressure and then, as the temperature increased to 1100 °C, a first GaN buffer layer with a thickness of 1100 nm was grown. After that, a second GaN buffer layer with a thickness of 1100 nm was grown

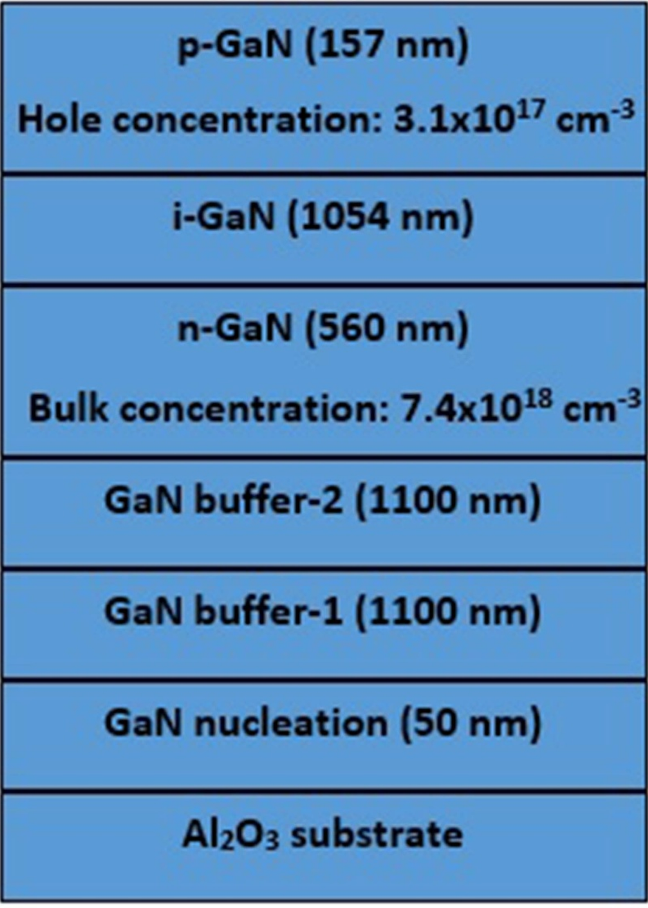

Figure 1. Cross-sectional structure of the GaN-based betavoltaic sample grown by MOCVD.

at 1100 °C and 200 mbar pressure. Then, an n-type GaN (Si:GaN) with a thickness of 560 nm while the TMGa resource flow was 10 sccm, SiH_4 was 20 sccm, and NH_3 was 2000 sccm; an i-GaN with a thickness of 1054 nm while the TMGa resource flow was 17 sccm and NH_3 was 1450 sccm; and a p-GaN (Mg:GaN) with a thickness of 157 nm at 1050 °C and 200 mbar pressure while the TMGa resource flow was 8 sccm, Cp_2Mg was 100 sccm, and NH_3 was 1300 sccm were consecutively grown. The cross-section of the GaN-based betavoltaic sample is shown in figure 1.

Referring to the studies in the literature [9, 25], in order to increase the lattice match in our epitaxial structure, to reduce the formation of defects and to increase the crystal quality, a nucleation layer was first formed on the substrate. Then, the two-stage buffer layer was enlarged to fill the gaps originating from the lower layers, and the impurities from the lower layers were prevented from deteriorating the crystal quality of the upper active layers. In order for the nuclear beta source (electrons from SEM in our study) to generate as much collision/scattering as possible, the i-GaN layer, which is the active layer to absorb the beta radiation, was kept thicker. However, considering the crystal quality, the p-GaN layer was kept thicker in order to increase the carrier collection capacity.

After the GaN-based p-i-n betavoltaic structure was grown, Mg activation was performed in a tube furnace with a N–air

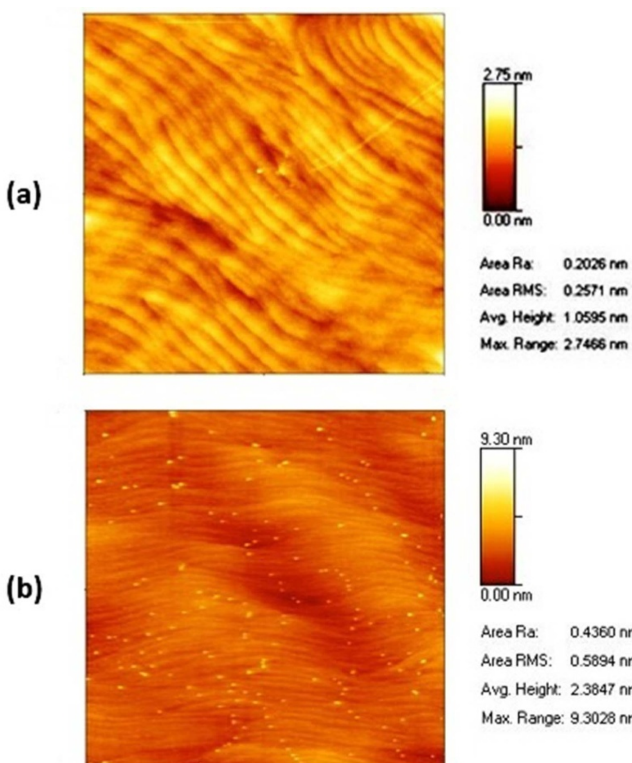

Figure 2. Typical AFM images of a 4×4 μm^2 area of (a) n-GaN surface and (b) p-GaN surface.

atmosphere at 830 °C for 15 min. A bulk carrier density of 7.39×10^{18} cm^{-3} for n-GaN and 1.03×10^{16} cm^{-3} for i-GaN, and a hole concentration of 3.06×10^{17} cm^{-3} for p-GaN, were measured using a Hall effect measurement system. Surface roughness measurements of n-GaN and p-GaN were performed in an atomic force microscope (AFM) and ascertained as 0.26 nm for n-GaN and 0.59 nm for p-GaN (figure 2).

The 2″ sample was cut into 12×12 mm^2 pieces for studies. Priorto the fabrication process, the samples were prepared by an organic cleaning procedure, using acetone, isopropanol and deionized water. Suss Microtec MA6 mask aligner was used for optical lithography, and AZ5214E photoresist was used for masking. Metal evaporation and ohmic annealing processes were performed in a Leybold Univex 350 electron beam evaporator system and Solaris 100 Rapid Thermal Annealing system, respectively. Ni with a Au cap layer is a popular ohmic contact for p-GaN, but the mechanism of annealing is still a controversial issue [21]. In addition, although there are many contact studies on p-GaN in the literature, the mentioned contacts may not be compatible with the epitaxial structure or may give very different results than expected. Hence, we investigated how various metal ratios of Ni/Au in a one-to-one N_2:O_2 (1:1) gas atmosphere depending on the temperature and different surface treatments affect the ohmic behavior of our structure. This systematic study is intended to guide studies to be done in this field. After finding a good ohmic contact for p-GaN, betavoltaic batteries were fabricated and DC characterized. To characterize these devices, a Raith SEM system was used as the electron source because of the difficulty of finding a nuclear beta source and of the procedures required to work. A printed circuit board (PCB) was designed and the devices were tested in the SEM. In this way, we attempted to maximize the performance of betavoltaic epitaxial structures before using a nuclear beta source.

The fabrication process for betavoltaic batteries started with etching to form an n-contact layer. A Suss Microtec MA6 mask aligner and AZ5214E photoresist were used for optical patterning of the n-contact regions of the devices. n-contact etching was performed with a Sentech inductively coupled plasma (ICP) reactive ion etching (RIE) system using Cl_2 (20 sccm)/BCl_3 (25 sccm)/Ar (10 sccm) plasma-based dry etch. The RF power, ICP power, chamber pressure, and cathode temperature were 100 W, 800 W, 0.4 Pa, and 20 °C, respectively. The entire p-GaN and i-GaN layers and 300 nm part of the n-GaN layer in the patterned regions were etched. A Ti (12 nm)/Al (120 nm)/Ni (35 nm)/Au (65 nm) metal stack was deposited and annealed in a N atmosphere at 875 °C for 30 s for the n-contact layer. Using the best conditions obtained in this study, p-contact layers were deposited with a Ni/Au metal stack and annealed. Then, a Ti (50 nm)/Au (350 nm) metal stack was deposited as a touch layer. After this step, a 100 nm p-GaN layer was etched in order to increase the particle penetration into the active layer. Then, a mesa etching with a depth of 600 nm was done for device isolation. A 300 nm SiO_2 layer was deposited as a surface passivation layer using plasma enhanced chemical vapor deposition (PECVD) using SiH_4 (50 sccm)/N_2O (70 sccm)/Ar (600 sccm) with an RF power of 140 W, cathode temperature of 250 °C, and chamber pressure of 210 Pa. Electrical contact openings were performed with a SAMCO ICP RIE system using SF_6 (4 sccm)/Ar (20 sccm) plasma-based dry etch with an RF power of 40 W, ICP power of 60 W, and chamber pressure of 0.6 Pa. Finally, a Ti (200 nm)/Au (2000 nm) metal stack was deposited as an interconnection, and the fabrication process was completed with this last step. Figure 3 shows a cross-sectional representation and optical microscope image of the fabrication completed GaN-based betavoltaic devices.

DC characterization of GaN-based betavoltaic devices was performed using a Keysight B1500A semiconductor device parameter analyzer.

A PCB was designed for electron susceptibility tests of the fabricated devices, and the connections of the betavoltaic devices on the 12×12 mm^2 sample were made to this PCB. Figure 4 shows the sample and devices on it with PCB connections.

DC measurements were taken from the PCB connected devices placed in the SEM with the help of a Keithley 2612. A schematic view of the measurement setup and SEM image of the betavoltaic device are given in figure 5.

3. Results

Before producing GaN-based betavoltaic devices, studies were carried out to obtain a good ohmic contact on the p-GaN layer of our epitaxial structure. For this, first, the effect of different Ni/Au metal ratios on the p-GaN ohmic behavior at an optimum temperature value of 500 °C for 5 min obtained from the literature in a one-to-one N_2/O_2 gas atmosphere was

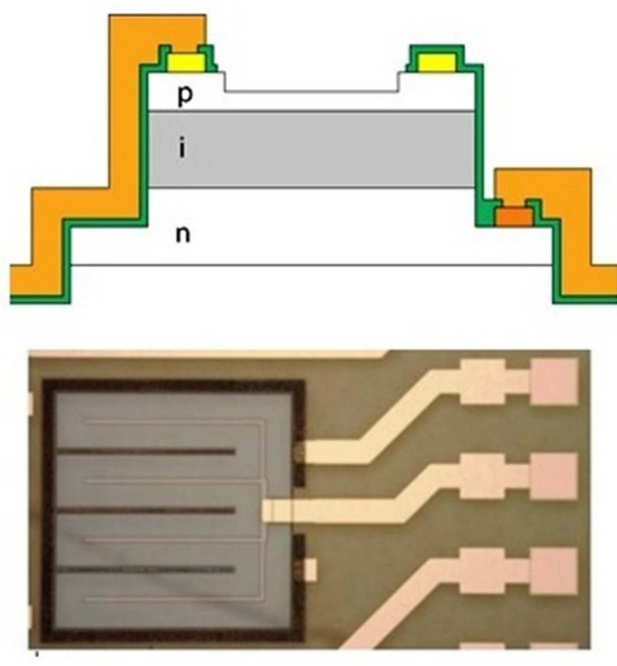

Figure 3. Cross-sectional representation and optical microscope image of the fabrication completed GaN-based betavoltaic devices.

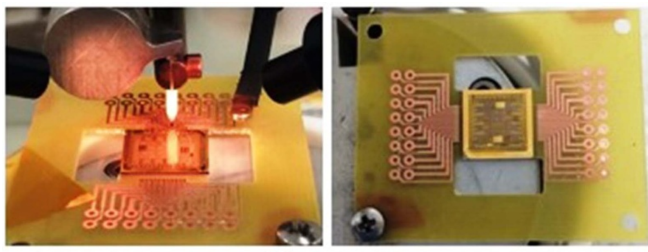

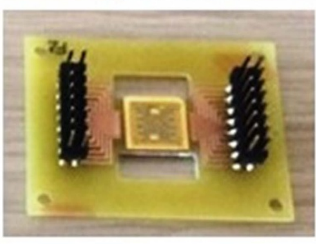

Figure 4. Sample of finished process, attached to PCB and wire bonded.

investigated. The transfer length method (TLM) measurement results obtained are shown in table 1 for annealing temperature of 500 °C, annealing time of 5 min and annealing atmosphere of N_2:O_2 (1:1).

When table 1 is examined, it is seen that ohmic properties could not be obtained for the F1 and F2 samples. Hence, to see the effect of temperature on these samples, new sample groups were prepared and the ohmic property was investigated at various temperature values. The TLM measurement results obtained are shown in table 2 for the same annealing atmosphere of N_2:O_2 (1:1), but different annealing temperatures and annealing times.

When table 2 is examined, it is seen that the F1 and F5 sample groups do not exhibit ohmic behavior for our epitaxial

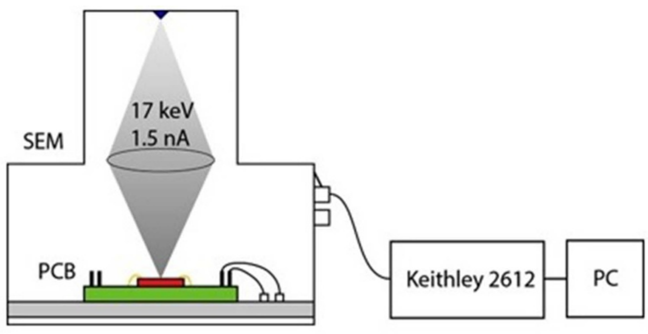

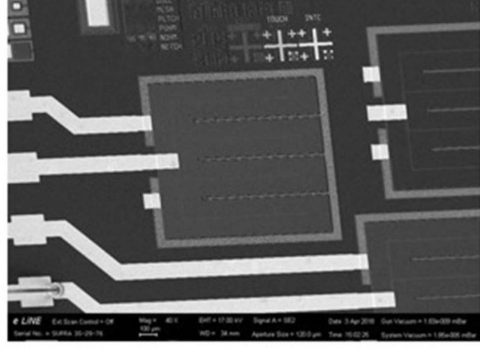

Figure 5. Schematic view of the measurement setup and SEM image of the betavoltaic devices.

Table 1. Summary of the TLM measurement results of different Ni/Au metal ratios on the p-GaN layer.

Sample	Ni/Au rations (nm/nm)	Specific contact resistivity (ohm·cm^2)
F1	3/3	No ohmic property
F2	5/5	0.88
F3	8/10	0.38
F4	25/20	2.81
F5	30/150	No ohmic property

[a] Annealing temperature: 500 °C.
[b] Annealing time: 5 min.
[c] Annealing atmosphere: N_2:O_2 (1:1).

structure. Thereupon, new sample groups were prepared based on the metal ratios in the F3 sample, which exhibits the best ohmic behavior in table 1. The effects of annealing temperature on ohmic behavior were also investigated for these sample groups. The TLM measurement results obtained are shown in table 3 for the same annealing atmosphere of N_2:O_2 (1:1), metal ratios of Ni/Au (8 nm/10 nm) and annealing time of 5 min, but different annealing temperatures.

When table 3 is examined, it is seen that the most suitable specific contact resistivity for our p-GaN layer is obtained after annealing the Ni/Au (8 nm/10 nm) metal stack at 500 °C for 5 min. For this sample, the *I–V* characteristic versus contact spacing and TLM measurement as a resistance versus contact spacing are shown in figures 6 and 7, respectively.

Using a Ni/Au (8 nm/10 nm) metal stack annealing at 500 °C process parameters, some surface chemical treatments were applied in order to lower the specific contact

Table 2. Summary of the TLM measurement results of different annealing temperatures and annealing times for the F1 and F5 sample groups.

Sample	Annealing temperature@Time	Specific contact resistivity (ohm·cm^2)
F1/F5	400 °C@1 min	No ohmic property
F1/F5	500 °C@1 min	No ohmic property
F1/F5	600 °C@1 min	No ohmic property
F1/F5	700 °C@1 min	No ohmic property
F1/F5	850 °C@1 min	No ohmic property
F1/F5	400 °C@5 min	No ohmic property
F1/F5	500 °C@5 min	No ohmic property
F1/F5	600 °C@5 min	No ohmic property
F1/F5	400 °C@10 min	No ohmic property
F1/F5	500 °C@10 min	No ohmic property

[a] Annealing atmosphere: N_2:O_2 (1:1).

Table 3. Summary of the TLM measurement results of different annealing temperatures for F3 sample groups.

Annealing temperature	Specific contact resistivity (ohm·cm^2)
400 °C	No ohmic property
470 °C	0.74
500 °C	0.38
550 °C	0.72
600 °C	2.5

[a] Ni/Au (8 nm/10 nm).
[b] Annealing atmosphere: N_2:O_2 (1:1).
[c] Annealing time: 5 min.

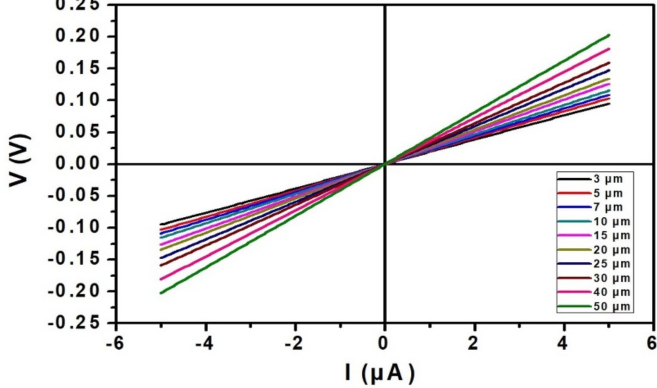

Figure 6. *I*–*V* characteristics versus contact spacing for the sample with a Ni/Au (8 nm/10 nm) metal stack annealing at 500 °C.

resistivity. Before p-contact layer lithography, one sample was exposed to a K-based buffered developer (AZ 400K Developer@MicroChemicals) with a temperature of 110 °C and the other with HCl (37%) at room temperature for 5 min, after which the samples were washed with DI water and dried with N_2 gas. After these procedures, p-contact lithographies were performed and Ni/Au p-contact coatings were done. The applied chemical treatments to the p-GaN layer before forming a p-contact layer and the TLM measurement results are shown in table 4 for the same annealing temperature of 500 °C, annealing time of 5 min and annealing atmosphere of N_2:O_2 (1:1).

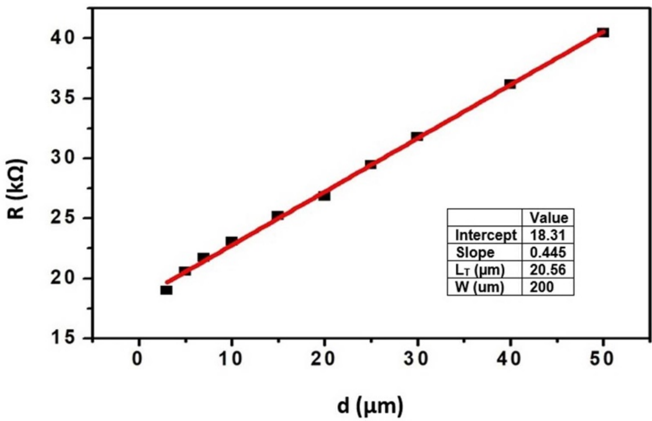

Figure 7. TLM measurement as a resistance versus contact spacing for the sample with a Ni/Au (8 nm/10 nm) metal stack annealing at 500 °C.

Table 4. Summary of the TLM measurement results of the applied chemical treatments to the p-GaN layer before forming a p-contact layer.

Chemical treatments	Specific contact resistivity (ohm·cm^2)
HCl (37%)	25.8
K-based buffered developer (AZ 400K Developer@ MicroChemicals)	0.06

[a] Ni/Au (8 nm/10 nm).
[b] Annealing atmosphere: N_2:O_2 (1:1).
[c] Annealing time: 5 min.

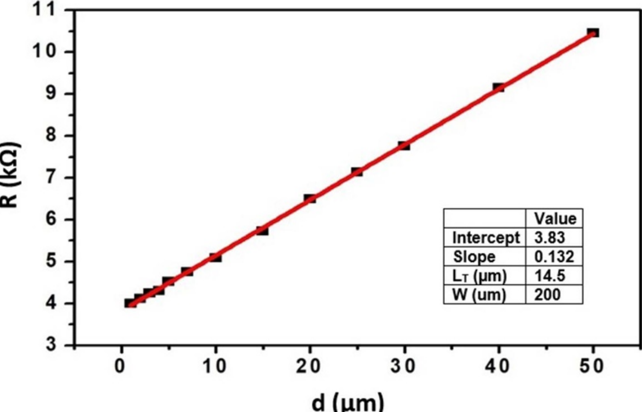

Figure 8. TLM measurement as a resistance versus contact spacing for the sample using a K-based buffered developer (AZ 400K Developer@MicroChemicals) as a surface chemical treatment before p-contact lithography.

When table 4 is examined, it is seen that the most suitable specific contact resistivity for our p-GaN layer is obtained when using a K-based buffered developer (AZ 400K Developer@MicroChemicals) as a surface chemical treatment before p-contact lithography. For this sample, the TLM measurement as a resistance versus contact spacing is shown in figure 8.

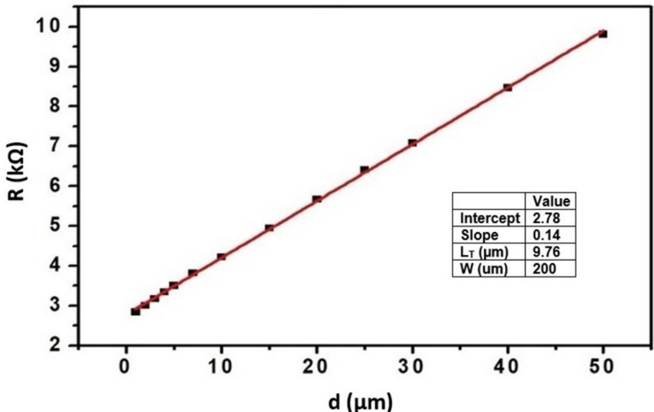

Figure 9. TLM measurement as a resistance versus contact spacing for the O_2 plasma treated sample.

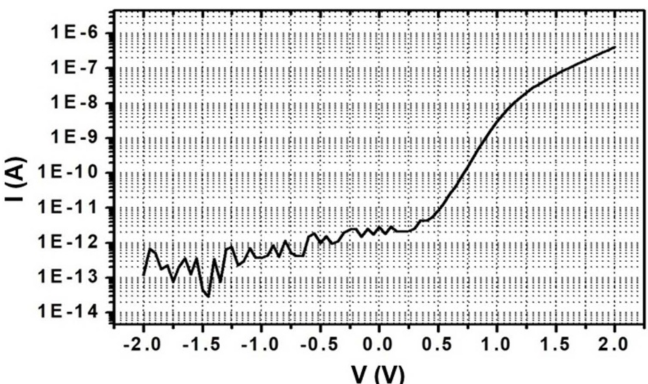

Figure 10. *I–V* characteristics of the betavoltaic devices under darkness.

After these surface chemical treatment processes, two more samples were prepared to see how an O_2 plasma treatment after p-contact lithography would change the p-contact specific contact resistivity. After a standard cleaning process and chemical surface treatment with a K-based buffered developer were applied to both samples, p-contact lithographies were performed. Then, plasma treatment was performed for 3 min for one of the samples using the AutoGlow plasma cleaning system using O_2 with RF power of 90 W and chamber pressure of 1 mbar, after which Ni/Au coating and annealing of the samples were performed. The specific contact resistivity value for the O_2 plasma treated sample was calculated as 0.027 ohm·cm^2. The TLM measurement graph for resistance versus contact spacing is shown in figure 9.

After obtaining an acceptable specific contact resistivity value for the p-GaN layer, GaN-based betavoltaic devices were fabricated. *I–V* characteristics of the betavoltaic devices under darkness and the electron beam from the SEM are shown in figures 10 and 11, respectively. The energy of the electrons sent with the help of the SEM was adjusted to match the energy of the particles emitted from a ^{63}Ni nuclear beta source.

The leakage currents of the betavoltaic devices in the dark are 0.12 pA at −2 V, 2.8 pA at 0 V, 8.4 pA at 0.5 V, and 3 nA at 1.0 V, respectively for the 1 × 1 mm^2 devices. The open-circuit voltage (V_{oc}) and short-circuit current (I_{sc}) of the devices under the electron beam with energy of 17 keV from the SEM are 1.9 V and 1.5 μA, respectively, as shown in figure 11.

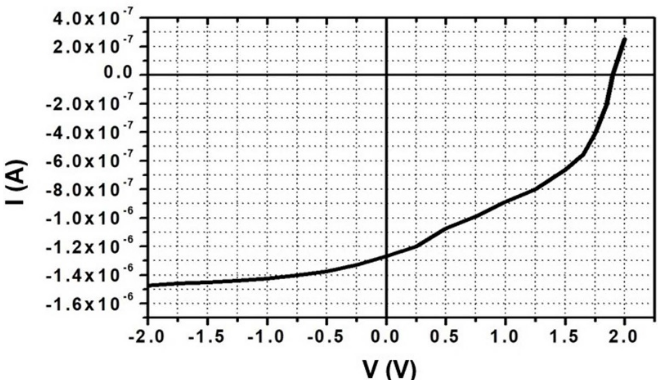

Figure 11. *I–V* characteristics of the betavoltaic devices under the electron beam from the SEM.

The electron current value (1.5 nA) sent to the sample is about 9.44 × 10^9 e$^-$ s^{-1}, which means that 100 times more beta particles are sent over the device compared to the 1 mCi (3.7 × 10^7 decay s^{-1}) value. However, the electron beam is not sent directly to the entire 1 × 1 mm^2 sample surface, but only to an area of 20 μm. The measured voltage (V_{max}) and current (I_{max}) at the maximum output power ($P_{out\text{-}max}$) of 1 μW are 1.25 V and 0.8 μA, respectively. The filling factor ($V_{max} \times I_{max}/V_{oc} \times I_{sc}$) and the maximum power conversion efficiency (maximum output power ($P_{out\text{-}max}$)/electron beam power to which the device is exposed (P_{source})) are 0.35 and 3.9%, respectively.

4. Conclusion

In this study, we designed our epitaxial structure within the scope of betavoltaic studies and developed a p-contact process in accordance with our own p-GaN layer. By removing H contamination and an amorphous native oxide layer with carbon/hydrocarbon contaminations on the p-GaN surface [22] with the surface chemical and plasma treatments we applied, we reduced our p-contact specific contact resistivity from 0.38 ohm·cm^2 to 0.027 ohm·cm^2. When this value is compared with the literature [9], it is a very good value. In addition, considering the difficulty of working with a nuclear source, we tested our first devices in this way, proposing to use SEM as an electron source instead of a beta source in order to accelerate developments in the field of betavoltaics. For our 1 × 1 mm^2 GaN-based betavoltaic devices, dark current, V_{oc}, I_{sc}, FF, efficiency, and $P_{out\text{-}max}$ were obtained as 2.8 pA at 0 V, 1.9 V, 1.5 μA, 0.35, 3.9%, and 1 μW, respectively. When the values were examined, it was seen that our fill factor (FF) value was lower than in the studies in the literature, but the efficiency was high [9]. A low FF value indicates that the series resistance in our device is high and a part of the obtained current is released as heat. For this purpose, it shows that we need to

conduct development studies both to reduce our p-contact resistance and to reduce our epitaxial layer resistances. In order to increase efficiency, we will continue our work by making some adjustments to our epitaxial structure and producing a higher quality epitaxial structure. After producing the devices with maximum FF and efficiency that we will obtain as a result of the test processes using SEM, we will test these devices with a real nuclear beta source and test whether the correlation works properly.

We believe that this study will be a guiding study not only in the development of nuclear betavoltaic devices but also in space applications, such as directing high-energy particles from the Sun and obtaining energy from them.

Data availability statement

All data that support the findings of this study are included within the article (and any supplementary files).

Acknowledgments

One of the authors (E O) acknowledges partial support from the Turkish Academy of Sciences. The authors would like to acknowledge Mustafa Öztürk, M Deniz Çalışkan and Bayram Bütün for their valuable support.

ORCID iDs

A Toprak https://orcid.org/0000-0003-4879-8296
D Yılmaz https://orcid.org/0000-0001-6102-4477

References

[1] He J, Cheng W-C, Wang Q, Cheng K, Yu H and Chai Y 2021 *Adv. Electron. Mater.* **7** 2001045
[2] Waltereit P *et al* 2012 *Phys. Status Solidi* a **209** 491–6
[3] Nakamura S, Senoh M, Nagahama S-I, Iwasa N, Yamada T, Matsushita T, Kiyoku H and Sugimoto Y 1996 *Appl. Phys. Lett.* **68** 2105
[4] Jia H, Guo L, Wang W and Chen H 2009 *Adv. Mater.* **21** 4641–6
[5] Duboz J, Laügt M, Schenk D, Beaumont B, Reverchon J-L, Wieck A D and Zimmerling T 2008 *Appl. Phys. Lett.* **92** 263501
[6] Grant J, Bates R, Cunningham W, Blue A, Melone J, McEwan F, Vaitkus J, Gaubas E and O'Shea V 2007 *Nucl. Instrum. Methods Phys. Res.* A **576** 60–5
[7] Razeghi M and Rogalski A 1996 *J. Appl. Phys.* **79** 7433–73
[8] Monroy E, Calle F, Pau J L, Muñoz E, Omnès F, Beaumont B and Gibart P 2001 *J. Cryst. Growth* **230** 537–43
[9] Cheng Z, Chen X, San H, Feng Z and Liu B 2012 *J. Micromech. Microeng.* **22** 074011
[10] Ehrenberg W, Lang C-S and West R 1951 *Proc. Phys. Soc.* A **64** 424
[11] Ohmart P E 1951 *J. Appl. Phys.* **22** 1504–5
[12] Adams T, Revankar S, Cabauy P, Elkind B and Cheu D 2016 *Nucl. Technol. Radiat. Prot.* **31** 356–60
[13] Prelas M A, Weaver C L, Watermann M L, Lukosi E D, Schott R J and Wisniewski D A 2014 *Prog. Nucl. Energy* **75** 117e148118
[14] Lu M, Zhang G-G, Fu K, Yu G-H, Su D and Hu J-F 2011 *Energy Convers. Manage.* **52** 1955–8
[15] Sciuto A, D'Arrigo G, Roccaforte F, Mazzillo M, Spinella R C and Raineri V 2011 *IEEE Trans. Electron. Devices* **58** 593–9
[16] Qiao Da Y, Chen X-J, Ren Y and Yuan W-Z 2011 *J. Microelectromech. Syst.* **20** 685–90
[17] Guo H *et al* 2003 *TRANSDUCERS '03 12th Int. Conf. on Solid-State Sensors, Actuators and Microsystems. Digest of Technical Papers (Cat. No. 03TH8664)* (https://doi.org/10.1109/SENSOR.2003.1215247)
[18] Blanchard J *et al* 2002 Board of regents of the University of Wisconsin System (US) *Technical Report* (https://doi.org/10.2172/799209)
[19] Xi S *et al* 2021 *Radiat. Eff. Defects Solids* **177** 213–29
[20] Cheng Z *et al* 2010 *2010 IEEE 5th Int. Conf. on Nano/Micro Engineered and Molecular Systems* (https://doi.org/10.1109/NEMS.2010.5592469)
[21] Li X *et al* 2007 *Proc. SPIE* **6471** 64711B
[22] Cao Y 2021 *Proc. Int. Conf. on Optoelectronic Materials and Devices (ICOMD 2021)* vol 12164
[23] Hull B A, Mohney S E, Venugopalan H S and Ramer J C 2000 *Appl. Phys. Lett.* **76** 2271
[24] Lu W, Aplin D, Clawson A R and Yu P K L 2013 *J. Vac. Sci. Technol.* A **31** 011502
[25] Khan M R, Smith J R, Tompkins R P, Kelley S, Litz M, Russo J, Leathersich J, Shahedipour-Sandvik F, Jones K A and Iliadis A 2017 *Solid State Electron.* **136** 24–29